Correlations between optical properties and Voronoi-cell area of quantum dots

Matthias C. Löbl [●],[1,*] Liang Zhai,[1] Jan-Philipp Jahn,[1] Julian Ritzmann,[2] Yongheng Huo,[3,4] Andreas D. Wieck,[2]
Oliver G. Schmidt,[3] Arne Ludwig,[2] Armando Rastelli,[5] and Richard J. Warburton[1]

[1]*Department of Physics, University of Basel, Klingelbergstrasse 82, CH-4056 Basel, Switzerland*
[2]*Lehrstuhl fur Angewandte Festkörperphysik, Ruhr-Universität Bochum, D-44780 Bochum, Germany*
[3]*Institute for Integrative Nanosciences, Leibniz IFW Dresden, Helmholtzstrasse 20, D-01069 Dresden, Germany*
[4]*Hefei National Laboratory for Physical Sciences at the Microscale (HFNL) & Shanghai Branch of the University of Science
and Technology of China (USTC), No.99, Xiupu Road, Pudong New District 201315, Shanghai, China*
[5]*Institute of Semiconductor and Solid State Physics, Johannes Kepler University Linz, Altenbergerstrasse 69, A-4040 Linz, Austria*

A semiconductor quantum dot (QD) can generate highly indistinguishable single photons at a high rate. For application in quantum communication and integration in hybrid systems, control of the QD optical properties is essential. Understanding the connection between the optical properties of a QD and the growth process is therefore important. Here, we show for GaAs QDs, grown by infilling droplet-etched nanoholes, that the emission wavelength, the neutral-to-charged exciton splitting, and the diamagnetic shift are strongly correlated with the capture-zone area, an important concept from nucleation theory. We show that the capture-zone model applies to the growth of this system even in the limit of a low QD density in which atoms diffuse over μm distances. The strong correlations between the various QD parameters facilitate preselection of QDs for applications with specific requirements on the QD properties; they also suggest that a spectrally narrowed QD distribution will result if QD growth on a regular lattice can be achieved.

I. INTRODUCTION

Semiconductor quantum dots (QDs) are excellent as a bright source of highly indistinguishable single photons [1–8] and entangled photon pairs [9–17]. A QD can host a single spin [18–21] which, however, has a too short coherence time for applications in quantum communication [22–25]. A hybrid system of a QD and an atomic quantum memory is more promising in that respect [26,27]. To connect a QD to an atomic memory based on rubidium, the QD should emit photons matched both in emission energy and bandwidth to the memory [28]. The emission energy can be matched by using GaAs QDs embedded in AlGaAs [29,30]; bandwidth matching can be achieved by using a Raman scheme [31–34].

The growth of QDs has been intensively studied employing scanning probe microscopy [35–43]. Aiming at entangled photon-pair generation, a connection between such an analysis and the optical properties [44–46] has focused mostly on the fine-structure splitting of the QD emission [47–54]. To tailor all the optical QD properties, it is important to understand how they are connected to the QD growth [37].

In this paper, we establish a strong correlation between the optical properties of GaAs QDs, such as emission energy and diamagnetic shift, and a basic concept from nucleation theory, the capture zone [42,55,56]. This correlation is not obvious since the applicability of the capture-zone model depends on conditions such as sudden nucleation [57] and spatially uniform diffusion [58]. Both are not necessarily fulfilled. The correlations that we find here are absent for InGaAs QDs [59] and locally very weak for SiGe QDs [42,58]. The system we investigate consists of GaAs QDs grown by infilling of Al-droplet-etched nanoholes in an AlGaAs surface [47,60].

We apply the capture-zone model to the first phase of this process, the formation and growth of Al droplets. The capture-zone model implies a correlation between Al-droplet volume (island size [42,61]) and capture-zone area. We show experimentally that this results in a strong correlation between the capture-zone area and the optical QD properties.

We use spatially resolved photoluminescence imaging to determine simultaneously the position and the optical properties of individual QDs. We investigate samples of low QD density where a QD is small relative to the distances between QDs (point-island model [56]). The capture zone of each QD is determined as its Voronoi cell (VC) [42,55,57,58]. From the distribution of the VC areas, we estimate a critical nucleus size of the Al droplets (see Appendix A). We find a strong negative correlation between the VC area (A_{VC}) of a QD and its emission energy, in turn, a strong positive correlation between A_{VC} and the diamagnetic shift of the emission. These results can be well explained with the capture-zone model describing the aggregation dynamics of the Al droplets. Correlations are measured for QDs of particularly low density $n_{QD} < 1\ \mu$m^{-2}, implying a diffusion length on the μm scale during the growth phase of Al droplets [43]. This is a striking result: The optical properties of a QD, which are directly related to its structure on an nm scale, are strongly correlated with its surroundings on a μm scale.
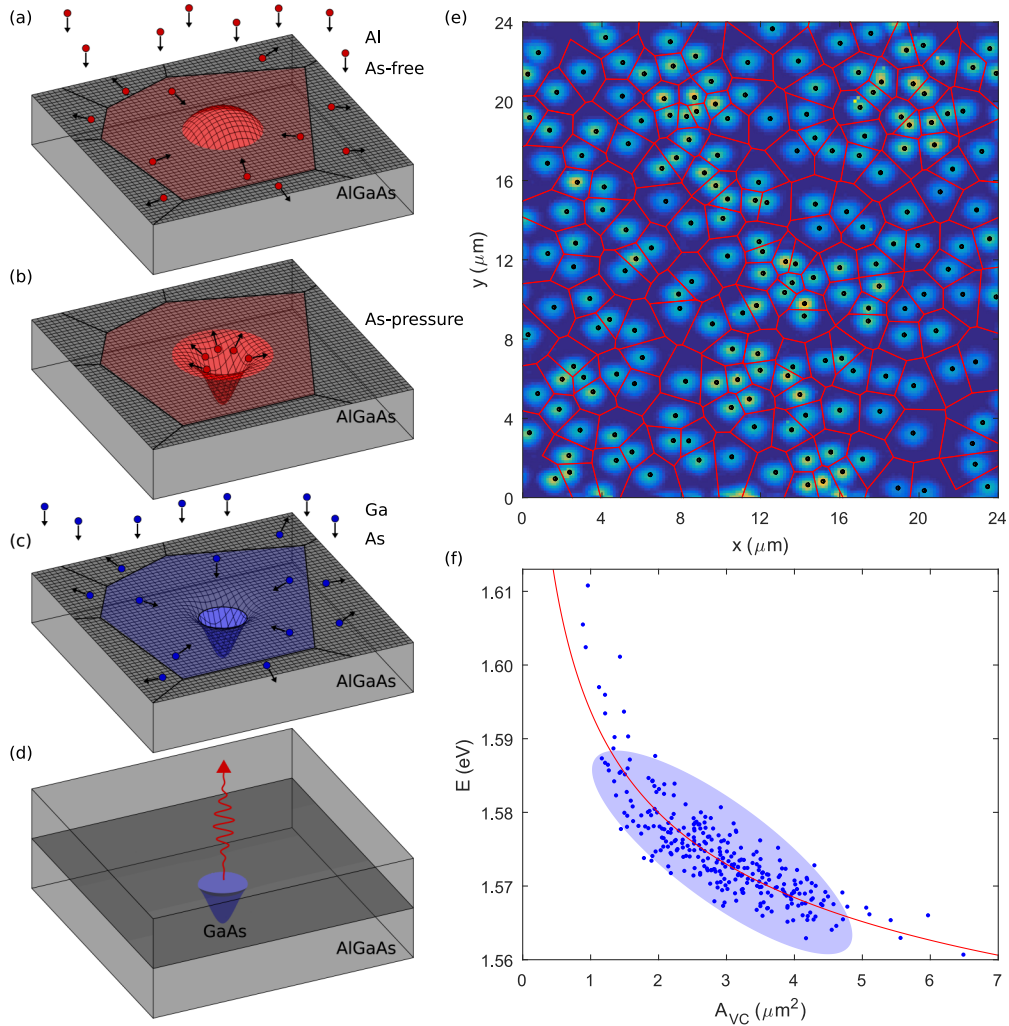
*matthias.loebl@unibas.ch

FIG. 1. (a) Schematic of the growth process of the quantum dots (QDs). In a first step, aluminum is deposited on an epitaxially grown AlGaAs surface. The aluminum atoms nucleate in the form of liquid nanodroplets. An atom is most likely to attach to the closest Al droplet. This is the Al droplet into whose capture zone (red area) the atom falls. (b) Underneath the Al droplet, the substrate material is unstable and nanohole etching takes place upon exposure to an arsenic flux. (c) After formation of nanoholes, GaAs is deposited. Diffusion leads to an infilling of the droplet-etched nanoholes with GaAs. (d) Finally, the sample is capped with AlGaAs. The GaAs within the nanohole is now embedded in higher band-gap AlGaAs and forms a QD. (e) Spatially resolved photoluminescence (PL) on a 24×24 μm^2-large region of sample A. Positions of individual QDs are obtained by Gaussian fitting (black dots). The red lines are the Voronoi cells (VCs) corresponding to the QD positions. (f) Relation between the VC area (A_{VC}) and the emission energy of the neutral exciton, X^0. The light-blue ellipse is a guide to the eye indicating the correlation in a linear approximation (correlation coefficient $\rho = -0.812$). The red line is a fit of Eq. (1).

II. SAMPLE GROWTH

The samples are grown by molecular-beam epitaxy (MBE) on a (001) substrate. We investigate two different samples (denoted here as A and B) that are grown in two different MBE chambers. QDs are grown by GaAs infilling of Al-droplet-etched nanoholes. A schematic depiction of the growth is shown in Fig. 1. First, aluminum is deposited on an AlGaAs surface in the absence of an As flux. The growth parameters are 0.5 ML on $Al_{0.4}Ga_{0.6}As$, $T = 600°$ C, flux $F = 0.5$ ML/s for sample A; and 0.16 ML on $Al_{0.33}Ga_{0.67}As$, $T = 630°$ C, flux $F = 0.18$ ML/s for sample B. For both samples, the layer thicknesses correspond to an equivalent amount of AlAs. The Al atoms nucleate (Volmer-Weber mode [62]) in the form of liquid nanodroplets on the sample surface [see Fig. 1(a)].

Underneath an Al droplet the substrate material is unstable leading to a nanoetching process [Fig. 1(b)] [60]. Under a low As flux, the etching proceeds until the whole Al droplet is consumed and the material is recrystallized in the surrounding region. Another 2 nm of GaAs are grown on top, filling up the nanoholes via diffusion during a 2-minute annealing step [Fig. 1(c)]. Overgrown with AlGaAs, the filled nanoholes become optically active QDs [Fig. 1(d)].

III. OPTICAL MEASUREMENTS

Optical measurements are performed in a helium bath cryostat. Photoluminescence (PL) is measured under above-band excitation ($\lambda = 633$ nm). An aspheric objective lens (NA = 0.68) collects the PL. The PL of the QD ensemble
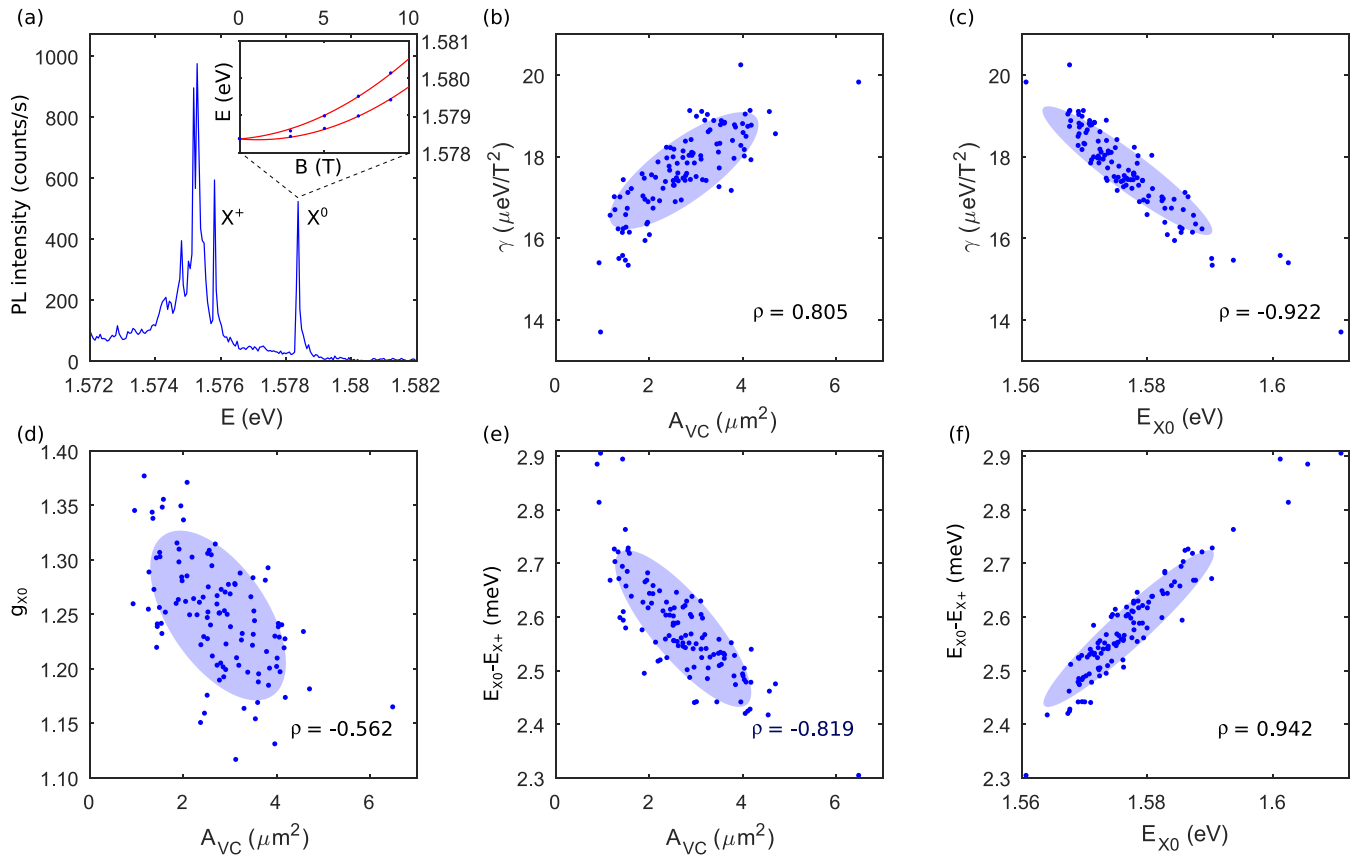
FIG. 2. (a) An exemplary PL spectrum of a QD. The emission line at the highest energy is the neutral exciton (X^0). At lower energy, emission of a singly charged exciton (X^+) and a broad emission from further excitons appear. The inset shows the X^0 emission energy as a function of the magnetic field. A diamagnetic shift and a Zeeman splitting are observed. The following subfigures refer to emission from X^0 on sample A. (b) Diamagnetic shift as a function of the Voronoi cell area, A_{VC} (correlation coefficient $\rho = 0.805$). The light blue ellipse has the same slope as a linear fit to the data points; its widths indicate a 1.5σ interval parallel and perpendicular to the slope. (c) Diamagnetic shift as a function of the emission energy of the neutral exciton. These parameters are negatively correlated ($\rho = -0.922$). (d) A weak correlation between the exciton g-factor and the Voronoi cell area, A_{VC}. (e) Splitting between neutral and positively charged excitons ($E_{X0} - E_{X+}$) as a function of A_{VC} ($\rho = -0.819$). (f) $E_{X0} - E_{X+}$ as a function of the X^0 emission energy ($\rho = 0.942$).

is centered at 787.4 nm for sample A, 798.0 nm for sample B (values referring to the neutral exciton X^0), with ensemble standard-deviations 3.4 and 1.4 nm, respectively. A typical spectrum of a single QD is shown in Fig. 2(a). The neutral exciton has the highest emission energy [29]; the positively charged exciton is redshifted by, on average, 2.7 meV (sample B: 2.1 meV). Additional exciton complexes appear at even lower energy [63], but are not the focus of our analysis.

Spatially resolved micro-PL is performed by scanning the sample with a low-temperature piezoelectric xy scanner (attocube ANSxy100/lr). A spatially resolved PL measurement is shown in Fig. 1(e). QDs can be identified as bright regions on this PL map. The lateral positions of the QDs are obtained by fitting two-dimensional Gaussians. A slight nonlinearity of the piezoscanner is corrected by using the widths of the fitted Gaussians as a reference (see Appendix B). We determine the capture zone around a QD by its Voronoi cell (VC) — the area that is closer to this particular QD than to any other one. A Voronoi diagram together with the corresponding QD positions is shown in Fig. 1(e). We find an average VC area of $\langle A_{VC} \rangle = 3.04 \pm 0.08$ μm^2 (sample A) and $\langle A_{VC} \rangle = 6.87 \pm 0.44$ μm^2 (sample B), corresponding to a QD density of $n_{QD} = 0.329 \pm 0.009$ μm^{-2} and $n_{QD} = 0.146 \pm 0.009$ μm^{-2}, respectively.

Shown in Fig. 1(f) is the emission energy of the neutral exciton E_{X^0} for many QDs as a function of the VC area, A_{VC}. The plot is obtained by combining three independent PL maps from sample A. We find a strong negative (Pearson) correlation coefficient of $\rho = -0.812$ (sample B: $\rho = -0.809$) between the emission energy and A_{VC} ($\rho = \pm 1$ maximum correlation; $\rho = 0$ no correlation). We explain this correlation by applying the capture-zone model to the growth phase of the Al droplets [Fig. 1(a)]. An Al atom, impinging at a random position on the sample, moves on the surface via diffusion and is most likely to attach to the closest Al droplet. In the capture-zone model, the growth rate of an Al droplet is thus assumed to be proportional to the VC area. If all Al droplets form at about the same time (sudden nucleation [57]), it leads to a correlation between Al-droplet volume and VC area. For an Al droplet with a small VC area, much material nucleates at its nearest neighbors, reducing its own accumulation rate. In turn, an Al droplet with a larger VC area accumulates more

atoms and the droplet-volume V_d becomes larger. For a larger Al droplet, the nanohole etched underneath it becomes deeper [37]. The QD subsequently formed from this nanohole has a weaker confinement in the growth direction, lowering its emission energy.

We obtain a quantitative relation between A_{VC} and the emission energy by the following considerations. In the capture-zone model, the volume of each Al droplet is proportional to A_{VC}. We assume that all Al droplets have a similar aspect ratio [51,64]. Then the droplet-height H_d is connected to the droplet-volume V_d and to the VC area by $H_d \propto V_d^{1/3} \propto A_{VC}^{1/3}$. For the relation between QD height H (nanohole depth, respectively) and the droplet-height H_d [37], we assume a phenomenological relation $H \propto H_d^{\beta}$. Since H is much smaller than the lateral extent of a QD [37], it is this parameter which mainly determines the emission energy of the QD. In the case of a hard-wall confinement and without considering Coulomb interaction terms, the emission energy of a QD is given by the bandgap plus electron and hole confinement energy: $E = E_0 + \frac{h^2}{8\mu H^2}$, where $E_0 = 1.519$ eV is the bandgap of the QD material (GaAs) and $\mu = (\frac{1}{m_e^*} + \frac{1}{m_h^*})^{-1}$ the reduced electron-hole effective mass ($m_e^* = 0.067 m_e$, $m_h^* = 0.51 m_e$). Including the $d = 2$ nm thick quantum well above the QDs leads to $E = E_0 + \frac{h^2}{8\mu(H+d)^2}$. Using the above relations one obtains an equation connecting A_{VC} and the emission energy E of the QD:

$$E = E_0 + \frac{h^2}{8\mu} \cdot ((\alpha \cdot A_{VC})^{\beta/3} + d)^{-2}. \quad (1)$$

A fit of Eq. (1) to the data is shown in Fig. 1(f). With the fit parameters $\alpha = 1.268 \times 10^{-32}$ m$^{3/\beta-2}$ and $\beta = 0.556$, we find a very good agreement with the data. The average height of a QD resulting from this fit is $H = 8.7$ nm which agrees well with AFM-measurements (see Appendix C). A direct correlation between the measured emission energy E_{X^0} and the term on the right-hand side of Eq. (1) shows an even higher correlation of $\rho = 0.879$ (see Appendix D) than that between emission energy and A_{VC}. This strong correlation supports our model for the connection between QD properties and capture zone.

We consider further QD properties and their connection to the VC area A_{VC}: the diamagnetic shift of the QD emission; and the splitting between neutral and positively charged exciton $E_{X^0} - E_{X^+}$. Both of these QD properties are connected mainly to the lateral rather than the vertical confinement of the QD.

We measure the energy of the PL emission (X^0) as a function of a magnetic field applied in the growth direction [inset to Fig. 2(a)]. The magnetic field splits the emission lines by the Zeeman energy and leads to a diamagnetic shift. For every QD we fit the relation [65,66]

$$E(B) = E(B = 0) + \gamma B^2 \pm \tfrac{1}{2} g \mu_B B, \quad (2)$$

where g is the exciton g-factor and μ_B the Bohr magneton. We approximate the diamagnetic shift with a parabola with prefactor γ [65,66]. The fine-structure splitting of the studied QDs [51] is negligibly small in this context. For the diamagnetic shift, a probe of the lateral area of the exciton, we find

values in the range $\gamma = 15$–20 μeV/T^2, in good agreement with Ref. [67]. The dependence of γ on the VC area (A_{VC}) is shown in Fig. 2(b). We find a correlation of $\rho = 0.805$ between A_{VC} and γ which reveals a connection between the capture-zone area and the lateral size of a QD. An Al droplet with a larger VC area has a larger lateral extent leading to a QD with a weaker lateral confinement potential. This finding is also fully compatible with the capture-zone model. For the direct dependence between the emission energy E_{X^0} and the diamagnetic shift γ, we find an approximately linear relation [Fig. 2(c)] associated with a correlation of $\rho = -0.922$. This connection between vertical and lateral confinement is consistent with a reported correlation between emission energy and s-to-p-shell splitting [63].

A plot of the exciton g-factor versus A_{VC} is shown in Fig. 2(d). The g-factor shows a slight dependence on A_{VC} with $\rho = -0.562$. For these QDs, the electron g-factor is very small such that the exciton g-factor is determined largely by the hole g-factor [31,67]. The hole states are predominantly heavy hole in character. However, even a small admixture of light-hole states reduces the g-factor from the heavy-hole limit by a large amount [68,69]. This light-hole admixture is size-dependent which can explain the dependence of the g-factor on A_{VC}. However, the g-factor is more weakly correlated with A_{VC} than the emission energy. We speculate that the hole g-factor is sensitive to the shape and not just the volume of the QD leading to a weaker correlation with A_{VC}.

Shown in Fig. 2(e) is the splitting between the neutral and the positively charged exciton ($E_{X^0} - E_{X^+}$) as a function of A_{VC}. Using single-particle wave functions, $E_{X^0} - E_{X^+}$ can be associated with the term $E_{eh} - E_{hh}$, where E_{hh}, E_{eh} are the direct Coulomb integrals between two holes and an electron and a hole, respectively [70,71]. Both terms decrease with increasing lateral size of the QD and hence with increasing size of the VC area A_{VC}. Experimentally, we observe a monotonic relation between A_{VC} and $E_{X^0} - E_{X^+}$ with a negative correlation ($\rho = -0.819$). For the direct relation between $E_{X^0} - E_{X^+}$ and the emission energy E_{X^0}, we find a linear dependence corresponding to a pronounced correlation of $\rho = 0.942$ [72] [see Fig. 2(f)]. This dependence also indicates a connection between the lateral and vertical confinements.

IV. CONCLUSION

We show how the optical properties of QDs grown by GaAs infilling of Al-droplet-etched nanoholes are connected to the capture-zone model, a concept from nucleation theory. The QD positions and the optical QD properties are obtained simultaneously by spatially resolved photoluminescence. The capture zone of QDs is determined by the Voronoi diagram of the QD positions. We find a strong negative correlation between the VC area and the emission energy of QDs. This result can be explained with the capture-zone model applied to the growth phase of the Al droplets. A relation between VC area and further optical properties (diamagnetic shift and neutral-to-charged exciton splitting) shows that not only the vertical but also the lateral QD size is correlated with the area of the capture zone. We measure these correlations on samples with low QD densities ($n_{QD} < 1$ μm^{-2}). Properties of a QD on a nm scale, which determine its optical emission, are therefore

connected to its surroundings on a μm scale. This result might be transferable to other nanostructures when strong material diffusion is present during the growth. The correlations between different QD parameters facilitate preselection of QDs for applications which place stringent requirements on the QD properties. The correlation between emission energy and capture-zone area has a powerful implication: If all capture-zone areas are made identical—e.g. by forcing the nucleation of the Al droplets on a lattice—then a spectrally narrow wavelength distribution of the QD ensemble can potentially be engineered. This idea has been successfully applied to stacked QD layers and QDs in pyramidal nanostructures [73–79]. For the system investigated here, Fig. 1(f) indicates that the QD ensemble would narrow by a factor of 2 if all Voronoi cell areas were in a range of 3–4 μm^2.

APPENDIX A: FREQUENCY DISTRIBUTION OF THE VORONOI CELL AREAS

The frequency distribution of the VC areas gives further information about the Al-droplet formation. The probability density distribution f_{VC} of the normalized VC areas $A_{VC}/\langle A_{VC} \rangle \equiv x$ is often modeled by a generalized Wigner distribution [80,81]:

$$f_{VC}(x \mid \eta) = a_\eta \cdot x^\eta \cdot \exp(-b_\eta x^2). \quad \text{(A1)}$$

In our notation, $f(x \mid \eta)$ corresponds to a probability density distribution for x under the condition η. The parameters b_η and a_η are defined by the constraint that f_{VC} is a normalized probability density distribution with a mean of 1. Explicit expressions for b_η, a_η are given in Refs. [82,83]. The parameter η can be connected to the critical nucleus size i, via $\eta \approx i + 2$ [81,83,84].

We fit Eq. (A1) to the distribution of normalized VC areas via likelihood optimization, without making approximations such as Poissonian or Gaussian error estimation [85]. Let

$\{A_{VC}^{(i)}\}_{i \in \{1,\dots,N\}}$ be the set of the areas corresponding to the N different Voronoi cells. We define $\{x^{(i)}\}_{i \in \{1,\dots,N\}}$ as the set of all normalized Voronoi cell areas, $x^{(i)} = A_{VC}^{(i)}/\langle A_{VC} \rangle$. Equation (A1) assigns a probability density to each value $x^{(i)}$. We assume that every value $x^{(i)}$ corresponds to an independent random variable $X^{(i)}$. Then, under the condition of a fixed value for η, the probability density of measuring a set of normalized Voronoi cells, $\{x^{(i)}\}_{i \in \{1,\dots,N\}}$, is given by

$$P\big(\{x^{(i)}\}_{i \in \{1,\dots,N\}} \big| \eta\big) = \prod_{i=1}^{N} f_{VC}(x^{(i)} \mid \eta). \quad \text{(A2)}$$

This likelihood distribution is maximum for $\eta = \eta_{opt} = 3.66$. The mean of the likelihood distribution is $\eta_m = 3.68$. The difference between mean and maximum of the likelihood distribution is small because the distribution is close to symmetric and only slightly biased. The found value of the parameter η corresponds to a critical nucleus size of $i \approx 2$.

The likelihood distribution, $P(\{x^{(i)}\}_{i \in \{1..N\}} \mid \eta)$, has a standard deviation of $\sigma_\eta = 0.33$ when varying η for a fixed measurement, $\{x^{(i)}\}_{i \in \{1,\dots,N\}}$. Bayes' theorem connects the probability density for measuring $\{x^{(i)}\}_{i \in \{1,\dots,N\}}$ under the condition of a fixed parameter η to the probability density for η under the condition of a measurement, $\{x^{(i)}\}_{i \in \{1,\dots,N\}}$:

$$P\big(\eta \big| \{x^{(i)}\}_{i \in \{1,\dots,N\}}\big) = \frac{P\big(\{x^{(i)}\}_{i \in \{1,\dots,N\}} \mid \eta\big) \cdot P(\eta)}{P\big(\{x^{(i)}\}_{i \in \{1,\dots,N\}}\big)}. \quad \text{(A3)}$$

The distribution $P(\{x^{(i)}\}_{i \in \{1,\dots,N\}})$ does not depend on η. Furthermore, we assume a uniform prior distribution $P(\eta)$. In this case, both probability density distributions $P(\eta \mid \{x^{(i)}\}_{i \in \{1,\dots,N\}})$ and $P(\{x^{(i)}\}_{i \in \{1,\dots,N\}} \mid \eta)$ are equal up to a prefactor which does not depend on η. Therefore, the width of both distributions is identical. The error on the parameter η is given by $\sigma_\eta = 0.33$, the standard deviation calculated for the likelihood distribution, $P(\{x^{(i)}\}_{i \in \{1,\dots,N\}} \mid \eta)$.

Shown in Fig. 3 is the distribution of the relative frequency f_{VC} of the normalized VC area $A_{VC}/\langle A_{VC} \rangle \equiv x$. In this figure, the normalized Voronoi cell areas, $\{x^{(i)}\}_{i \in \{1,\dots,N\}}$, are divided in finite intervals. The solid red line is the fit ($\eta = \eta_{opt} = 3.66$) of Eq. (A1) to the data, $\{x^{(i)}\}_{i \in \{1,\dots,N\}}$.
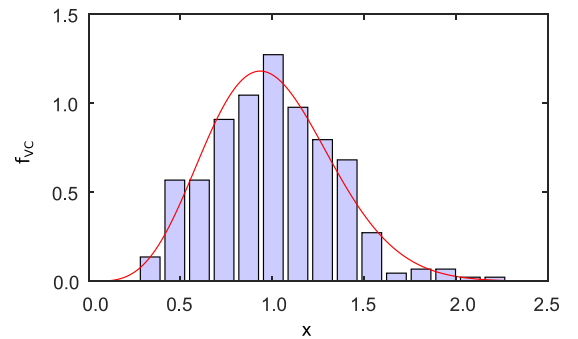

FIG. 3. Frequency distribution f_{VC} of the normalized Voronoi cell area, $A_{VC}/\langle A_{VC} \rangle \equiv x$. For better visibility, the normalized Voronoi cell areas are divided in finite intervals. The red line is a fit of Eq. (A1) obtained by likelihood optimization.
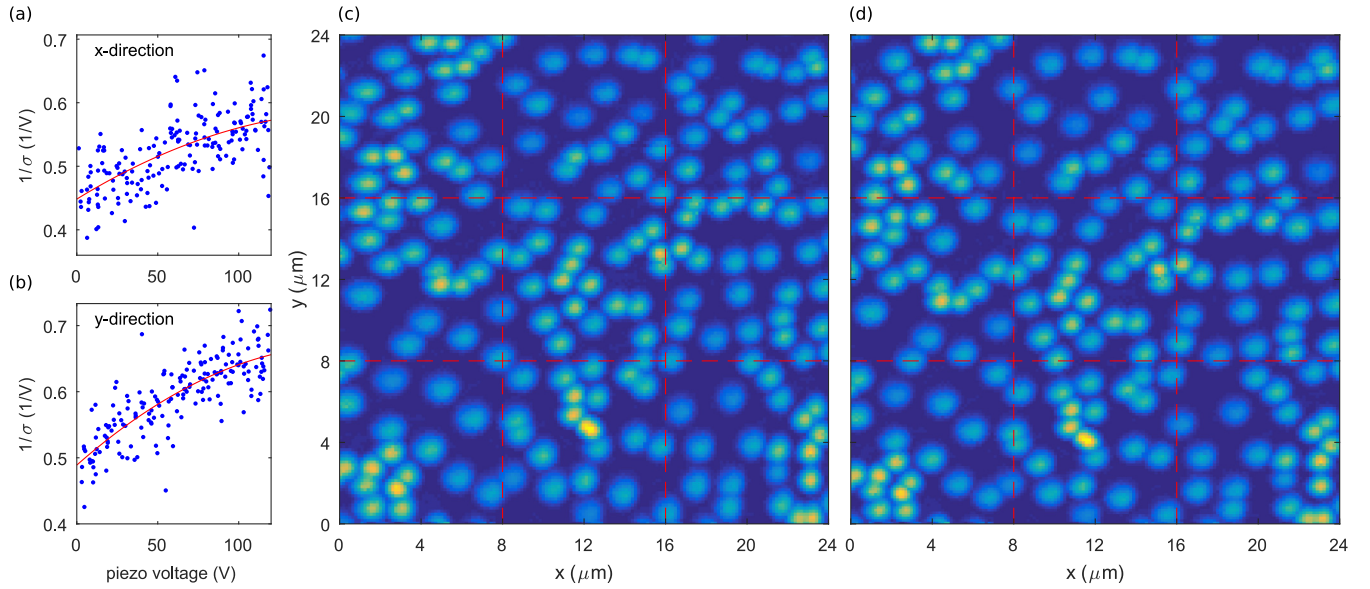
FIG. 4. Correction of the distortion due to the nonlinearity of the piezoscanners. The QD position is set by the voltages $V_{x/y}$ applied to the piezoscanners. The distortion correction is carried out independently for the (a) x and (b) y directions (x direction in the following explanation). Initially, the spot size σ_x is measured for every QD in units of the voltage applied to the piezoscanner. It is obtained by fitting a two-dimensional Gaussian to the PL intensity which is spectrally filtered to select individual QDs. For a larger derivative $\frac{dx}{dV_x}$, the spot size appears smaller than for a smaller value of $\frac{dx}{dV_x}$. The spot size σ_x is therefore inversely proportional to the derivative $\frac{dx}{dV_x}$. The red curves in (a), (b) are fits to a phenomenological parabolic dependence between applied piezovoltage V_x and $1/\sigma_x$: $\frac{dx}{dV_x} = \tilde{c}/\sigma_x = \tilde{c}(a_0 + a_1 V_x + a_2 V_x^2)$. We use the fit results to map V_x to the position $x(V_x) = \tilde{c} \int_0^{V_x} (a_0 + a_1 V + a_2 V^2)\, dV$. The prefactor $\tilde{c}$ is obtained by the constraint that the highest voltage corresponds to the full scan range. (c) PL intensity as a function of the xy position. The PL is integrated over the full QD ensemble. The PL map is shown without the distortion correction assuming that position and applied piezovoltage are related linearly. Due to the described nonlinearity of the piezoscanners, the QD spots at low voltages appear slightly larger in comparison to the QD spots at high voltages — the PL map is distorted. (d) The same PL map with a distortion correction using the above method. The QD spot sizes are homogeneous, indicating a successful correction of the distortion.
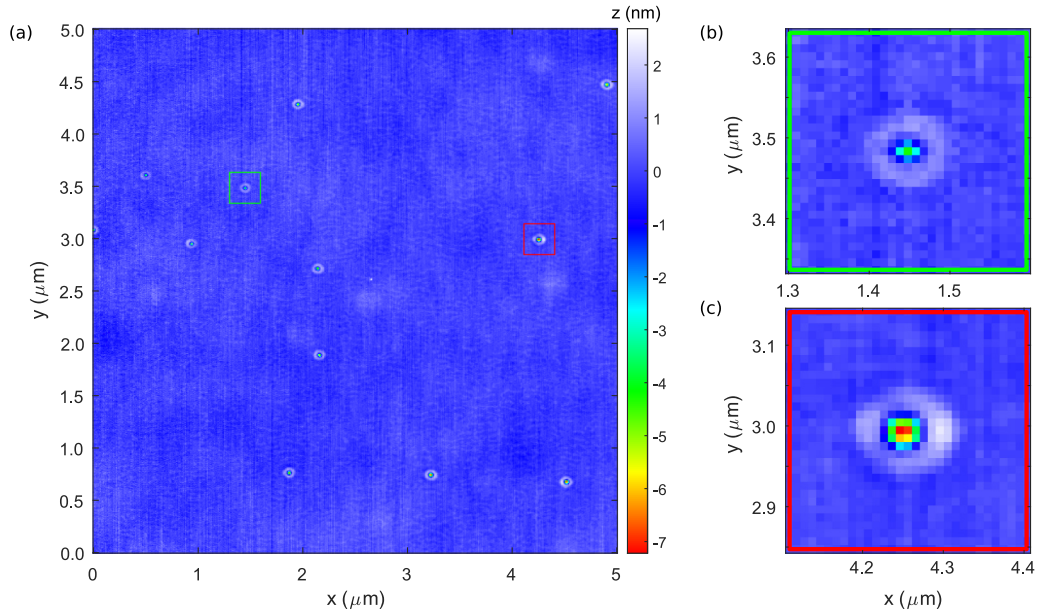

FIG. 5. (a) An atomic force microscopy (AFM) image on a sample similar to sample A. The growth is stopped after etching the nanoholes. The size of the AFM scan is $5 \times 5~\mu\text{m}^2$ with 512×512 pixels. The AFM image indicates that the more separated nanoholes (with a larger VC area) are deeper than those with a close-by neighbor. This finding is in good agreement with the results shown in the main text. A zoom-in of two nanoholes is shown in (b, c) to illustrate this observation. The first nanohole has several close-by neighbors and is shallow. In contrast, the second nanohole is more isolated and is particularly deep. The image size and resolution are too low to allow for a quantitative statistical analysis comparable to the main text. Note that an AFM image comparable in size to the presented PL measurements, simultaneously imaging individual nanoholes with ~ 2 nm resolution, would have to be $\sim 10^4 \times 10^4$ pixels large — a very time-consuming measurement.

APPENDIX B: CORRECTION OF THE NONLINEARITY OF THE PIEZOSCANNERS

The determination of Voronoi cell sizes is based on measuring the PL as a function of the position. Such a PL map is carried out by scanning the sample position with piezelectric *xy* scanners. The scanners have a hysteresis which, however, does not affect our measurements as we perform all measurements while scanning in the forward direction. Besides, the piezoscanner position depends nonlinearly on the applied voltage. This nonlinearity could potentially be corrected by calibrating the piezoscanners with a well-defined reference-structure. Here, we use a different approach: The emission spot of a QD appears differently in size depending on the absolute position of the scanner. The QD spot size is a direct measure of the nonlinear dependence between the applied piezovoltage and the position. The lateral size of a QD itself (<40 nm) is negligible in comparison to the spot size. We can, therefore, use the widths of the QD spots as a reference to compensate for the distortion of the PL map. The corresponding procedure is explained in the caption of Fig. 4. The distortion correction works well due to the large number of QDs on each PL map. A comparison of a PL map with and without distortion correction is shown in Figs. 4(c) and 4(d).

APPENDIX C: AFM MEASUREMENT

We perform an AFM measurement on a reference sample for which the growth is stopped after etching of the nanoholes. An AFM image of a 5×5 μm^2 large region is shown in Fig. 5. The measurement suggests that nanoholes with other nanoholes in their proximity are shallower in comparison to more separated ones. This finding is consistent with the capture-zone model and the results obtained by spatially resolved photoluminescence. The size of the AFM image does not allow for a quantitative analysis comparable to which is done based on the spatially resolved PL measurements.

APPENDIX D: EMISSION ENERGY VS VORONOI CELL AREA

Shown in Fig. 6 is the dependence between the emission energy and the VC area, A_{VC}, for the two different samples (A, B). For both samples, we observe that the emission energy decreases with increasing VC area.
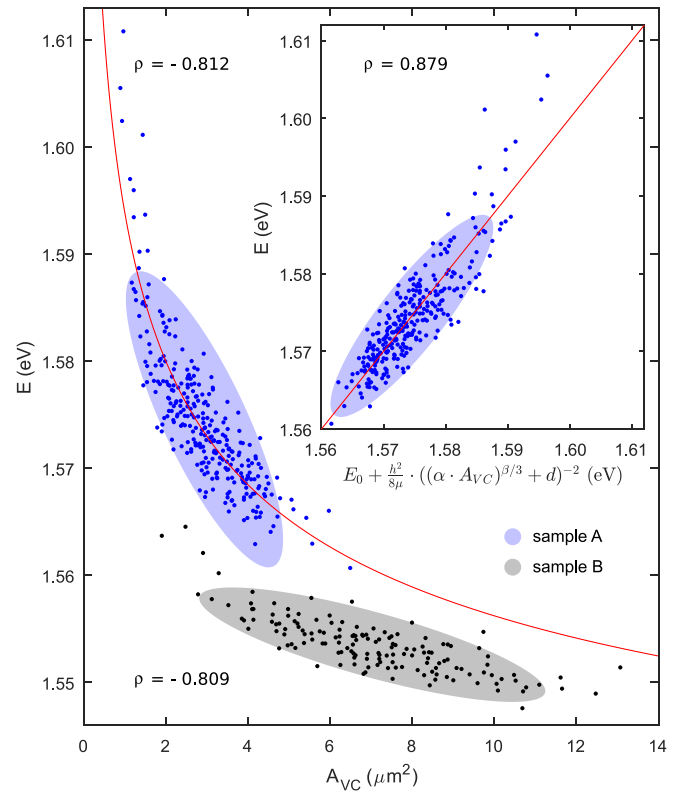

FIG. 6. Emission energy (X^0) as a function of Voronoi cell area (A_{VC}). The red line is a fit to Eq. (1) for QDs on sample A (blue points). Inset: Emission energy of QDs on sample A as a function of the expression on the right-hand side of Eq. (1). The relation between both quantities is more linear (correlation coefficient $|\rho| = 0.879$) than the direct relation of emission energy and A_{VC} ($|\rho| = 0.812$) which supports Eq. (1). QDs on sample B (black data points) are red-shifted compared to QDs on sample A.

Equation (1) suggests that the relation between A_{VC} and emission energy is nonlinear. In Fig. 6 we plot the emission energy as a function of the expression on the right-hand side of Eq. (1). The correlation of this dependence is higher ($|\rho| = 0.879$) than the correlation between emission energy and A_{VC} ($|\rho| = 0.812$). This result suggests that Eq. (1) is a better description of the data than a linear approximation.

[1] D. Huber, M. Reindl, Y. Huo, H. Huang, J. S. Wildmann, O. G. Schmidt, A. Rastelli, and R. Trotta, Nat. Commun. **8**, 15506 (2017).

[2] X. Ding, Y. He, Z.-C. Duan, N. Gregersen, M.-C. Chen, S. Unsleber, S. Maier, C. Schneider, M. Kamp, S. Höfling, C.-Y. Lu, and J.-W. Pan, Phys. Rev. Lett. **116**, 020401 (2016).

[3] N. Somaschi, V. Giesz, L. D. Santis, J. C. Loredo, M. P. Almeida, G. Hornecker, S. L. Portalupi, T. Grange, C. Antón, J. Demory, C. Gómez, I. Sagnes, N. D. Lanzillotti-Kimura, A. Lemaítre, A. Auffeves, A. G. White, L. Lanco, and P. Senellart, Nat. Photon. **10**, 340 (2016).

[4] G. Kiršanskė, H. Thyrrestrup, R. S. Daveau, C. L. Dreeßen, T. Pregnolato, L. Midolo, P. Tighineanu, A. Javadi, S. Stobbe, R. Schott, A. Ludwig, A. D. Wieck, S. I. Park, J. D. Song, A. V. Kuhlmann, I. Söllner, M. C. Löbl, R. J. Warburton, and P. Lodahl, Phys. Rev. B **96**, 165306 (2017).

[5] F. Liu, A. J. Brash, J. O'Hara, L. M. P. P. Martins, C. L. Phillips, R. J. Coles, B. Royall, E. Clarke, C. Bentham, N. Prtljaga, I. E. Itskevich, L. R. Wilson, M. S. Skolnick, and A. M. Fox, Nat. Nanotechnol. **13**, 835 (2018).

[6] Y.-M. He, J. Liu, S. Maier, M. Emmerling, S. Gerhardt, M. Davanco, K. Srinivasan, C. Schneider, and S. Höfling, Optica **4**, 802 (2017).

[7] M. Gschrey, A. Thoma, P. Schnauber, M. Seifried, R. Schmidt, B. Wohlfeil, L. Krüger, J. H. Schulze, T. Heindel, S. Burger,

F. Schmidt, A. Strittmatter, S. Rodt, and S. Reitzenstein, Nat. Commun. **6**, 7662 (2015).

[8] E. Schöll, L. Hanschke, L. Schweickert, K. D. Zeuner, M. Reindl, S. F. Covre da Silva, T. Lettner, R. Trotta, J. J. Finley, K. Müller, A. Rastelli, V. Zwiller, and K. D. Jöns, Nano Lett. **19**, 2404 (2019).

[9] R. M. Stevenson, R. J. Young, P. Atkinson, K. Cooper, D. A. Ritchie, and A. J. Shields, Nature **439**, 179 (2006).

[10] N. Akopian, N. H. Lindner, E. Poem, Y. Berlatzky, J. Avron, D. Gershoni, B. D. Gerardot, and P. M. Petroff, Phys. Rev. Lett. **96**, 130501 (2006).

[11] A. J. Hudson, R. M. Stevenson, A. J. Bennett, R. J. Young, C. A. Nicoll, P. Atkinson, K. Cooper, D. A. Ritchie, and A. J. Shields, Phys. Rev. Lett. **99**, 266802 (2007).

[12] Y. Chen, M. Zopf, R. Keil, F. Ding, and O. G. Schmidt, Nat. Commun. **9**, 2994 (2018).

[13] D. Huber, M. Reindl, S. F. Covre da Silva, C. Schimpf, J. Martín-Sánchez, H. Huang, G. Piredda, J. Edlinger, A. Rastelli, and R. Trotta, Phys. Rev. Lett. **121**, 033902 (2018).

[14] J. Liu, R. Su, Y. Wei, B. Yao, S. F. C. da Silva, Y. Yu, J. Iles-Smith, K. Srinivasan, A. Rastelli, J. Li, and X. Wang, Nat. Nanotechnol. **14**, 586 (2019).

[15] F. B. Basset, M. B. Rota, C. Schimpf, D. Tedeschi, K. D. Zeuner, S. F. C. da Silva, M. Reindl, V. Zwiller, K. D. Jöns, A. Rastelli, and R. Trotta, arXiv:1901.06646.

[16] H. Wang, H. Hu, T.-H. Chung, J. Qin, X. Yang, J.-P. Li, R.-Z. Liu, H.-S. Zhong, Y.-M. He, X. Ding, Y.-H. Deng, Q. Dai, Y.-H. Huo, S. Höfling, C.-Y. Lu, and J.-W. Pan, Phys. Rev. Lett. **122**, 113602 (2019).

[17] M. Zopf, R. Keil, Y. Chen, J. Yang, D. Chen, F. Ding, and O. G. Schmidt, arXiv:1901.07833.

[18] M. Atatüre, J. Dreiser, A. Badolato, A. Högele, K. Karrai, and A. Imamoglu, Science **312**, 551 (2006).

[19] A. Bechtold, D. Rauch, F. Li, T. Simmet, P.-L. Ardelt, A. Regler, K. Müller, N. A. Sinitsyn, and J. J. Finley, Nat. Phys. **11**, 1005 (2015).

[20] A. Javadi, D. Ding, M. H. Appel, S. Mahmoodian, M. C. Löbl, I. Söllner, R. Schott, C. Papon, T. Pregnolato, S. Stobbe, L. Midolo, T. Schröder, A. Dirk Wieck, A. Ludwig, R. J. Warburton, and P. Lodahl, Nat. Nanotechnol. **13**, 398 (2018).

[21] M. C. Löbl, I. Söllner, A. Javadi, T. Pregnolato, R. Schott, L. Midolo, A. V. Kuhlmann, S. Stobbe, A. D. Wieck, P. Lodahl, A. Ludwig, and R. J. Warburton, Phys. Rev. B **96**, 165440 (2017).

[22] J. H. Prechtel, J. H. A. V. Kuhlmann, A. Ludwig, S. R. Valentin, A. D. Wieck, and R. J. Warburton, Nat. Mater. **15**, 981 (2016).

[23] A. Delteil, Z. Sun, W. bo Gao, E. Togan, S. Faelt, and A. Imamoglu, Nat. Phys. **12**, 218 (2016).

[24] G. Éthier-Majcher, D. Gangloff, R. Stockill, E. Clarke, M. Hugues, C. Le Gall, and M. Atatüre, Phys. Rev. Lett. **119**, 130503 (2017).

[25] D. Ding, M. H. Appel, A. Javadi, X. Zhou, M. C. Löbl, I. Söllner, R. Schott, C. Papon, T. Pregnolato, L. Midolo, A. D. Wieck, A. Ludwig, R. J. Warburton, T. Schröder, and P. Lodahl, Phys. Rev. Applied **11**, 031002 (2019).

[26] N. Sangouard, C. Simon, J. Minář, H. Zbinden, H. de Riedmatten, and N. Gisin, Phys. Rev. A **76**, 050301(R) (2007).

[27] M. T. Rakher, R. J. Warburton, and P. Treutlein, Phys. Rev. A **88**, 053834 (2013).

[28] J. Wolters, G. Buser, A. Horsley, L. Béguin, A. Jöckel, J.-P. Jahn, R. J. Warburton, and P. Treutlein, Phys. Rev. Lett. **119**, 060502 (2017).

[29] J.-P. Jahn, M. Munsch, L. Béguin, A. V. Kuhlmann, M. Renggli, Y. Huo, F. Ding, R. Trotta, M. Reindl, O. G. Schmidt, A. Rastelli, P. Treutlein, and R. J. Warburton, Phys. Rev. B **92**, 245439 (2015).

[30] R. Keil, M. Zopf, Y. Chen, B. Höfer, J. Zhang, F. Ding, and O. G. Schmidt, Nat. Commun. **8**, 15501 (2017).

[31] L. Béguin, J.-P. Jahn, J. Wolters, M. Reindl, Y. Huo, R. Trotta, A. Rastelli, F. Ding, O. G. Schmidt, P. Treutlein, and R. J. Warburton, Phys. Rev. B **97**, 205304 (2018).

[32] B. C. Pursley, S. G. Carter, M. K. Yakes, A. S. Bracker, and D. Gammon, Nat. Commun. **9**, 115 (2018).

[33] J. P. Lee, L. M. Wells, B. Villa, S. Kalliakos, R. M. Stevenson, D. J. P. Ellis, I. Farrer, D. A. Ritchie, A. J. Bennett, and A. J. Shields, Phys. Rev. X **8**, 021078 (2018).

[34] Y. He, Y.-M. He, Y.-J. Wei, X. Jiang, M.-C. Chen, F.-L. Xiong, Y. Zhao, C. Schneider, M. Kamp, S. Höfling, C.-Y. Lu, and J.-W. Pan, Phys. Rev. Lett. **111**, 237403 (2013).

[35] A. Rastelli, S. Stufler, A. Schliwa, R. Songmuang, C. Manzano, G. Costantini, K. Kern, A. Zrenner, D. Bimberg, and O. G. Schmidt, Phys. Rev. Lett. **92**, 166104 (2004).

[36] D. M. Bruls, J. W. A. M. Vugs, P. M. Koenraad, H. W. M. Salemink, J. H. Wolter, M. Hopkinson, M. S. Skolnick, F. Long, and S. P. A. Gill, Appl. Phys. Lett. **81**, 1708 (2002).

[37] P. Atkinson, E. Zallo, and O. G. Schmidt, J. Appl. Phys. **112**, 054303 (2012).

[38] M. Fanfoni, F. Arciprete, C. Tirabassi, D. Del Gaudio, A. Filabozzi, A. Balzarotti, F. Patella, and E. Placidi, Phys. Rev. E **86**, 061605 (2012).

[39] C. Heyn, A. Stemmann, A. Schramm, H. Welsch, W. Hansen, and A. Nemcsics, Phys. Rev. B **76**, 075317 (2007).

[40] A. Rastelli, M. Stoffel, A. Malachias, T. Merdzhanova, G. Katsaros, K. Kern, T. H. Metzger, and O. G. Schmidt, Nano Lett. **8**, 1404 (2008).

[41] D. M. Nothern and J. M. Millunchick, J. Vac. Sci. Technol. B **30**, 060603 (2012).

[42] S. Miyamoto, O. Moutanabbir, E. E. Haller, and K. M. Itoh, Phys. Rev. B **79**, 165415 (2009).

[43] S. Bietti, C. Somaschini, L. Esposito, A. Fedorov, and S. Sanguinetti, Appl. Phys. Lett. **116**, 114311 (2014).

[44] A. Rastelli, R. Songmuang, and O. G. Schmidt, Physica E **23**, 384 (2004).

[45] A. Surrente, M. Felici, P. Gallo, A. Rudra, B. Dwir, and E. Kapon, Appl. Phys. Lett. **111**, 221102 (2017).

[46] L. Sapienza, J. Liu, J. D. Song, S. Fält, W. Wegscheider, A. Badolato, and K. Srinivasan, Sci. Rep. **7**, 6205 (2017).

[47] Y. H. Huo, A. Rastelli, and O. G. Schmidt, Appl. Phys. Lett. **102**, 152105 (2013).

[48] J. D. Plumhof, V. Křápek, L. Wang, A. Schliwa, D. Bimberg, A. Rastelli, and O. G. Schmidt, Phys. Rev. B **81**, 121309(R) (2010).

[49] M. Abbarchi, T. Kuroda, T. Mano, and K. Sakoda, J. Phys. Conf. Ser. **245**, 012049 (2010).

[50] L. O. Mereni, O. Marquardt, G. Juska, V. Dimastrodonato, E. P. O'Reilly, and E. Pelucchi, Phys. Rev. B **85**, 155453 (2012).

[51] Y. H. Huo, V. Křápek, A. Rastelli, and O. G. Schmidt, Phys. Rev. B **90**, 041304(R) (2014).

[52] X. Liu, N. Ha, H. Nakajima, T. Mano, T. Kuroda, B. Urbaszek, H. Kumano, I. Suemune, Y. Sakuma, and K. Sakoda, Phys. Rev. B **90**, 081301(R) (2014).

[53] J. Skiba-Szymanska, R. M. Stevenson, C. Varnava, M. Felle, J. Huwer, T. Müller, A. J. Bennett, J. P. Lee, I. Farrer, A. B. Krysa, P. Spencer, L. E. Goff, D. A. Ritchie, J. Heffernan, and A. J. Shields, Phys. Rev. Appl. **8**, 014013 (2017).

[54] F. Basso Basset, S. Bietti, M. Reindl, L. Esposito, A. Fedorov, D. Huber, A. Rastelli, E. Bonera, R. Trotta, and S. Sanguinetti, Nano Lett. **18**, 505 (2018).

[55] P. A. Mulheran and J. A. Blackman, Phys. Rev. B **53**, 10261 (1996).

[56] J. A. Blackman and P. A. Mulheran, Phys. Rev. B **54**, 11681 (1996).

[57] M. Fanfoni, E. Placidi, F. Arciprete, E. Orsini, F. Patella, and A. Balzarotti, Phys. Rev. B **75**, 245312 (2007).

[58] F. Ratto, A. Locatelli, S. Fontana, S. Kharrazi, S. Ashtaputre, S. K. Kulkarni, S. Heun, and F. Rosei, Phys. Rev. Lett. **96**, 096103 (2006).

[59] P. Spencer, C. Chen, W. Michailow, H. Beere, and D. Ritchie, arXiv:1906.05842.

[60] Z. M. Wang, B. L. Liang, K. A. Sablon, and G. J. Salamo, Appl. Phys. Lett. **90**, 113120 (2007).

[61] S. Pratontep, M. Brinkmann, F. Nüesch, and L. Zuppiroli, Phys. Rev. B **69**, 165201 (2004).

[62] C. Heyn, T. Bartsch, S. Sanguinetti, D. Jesson, and W. Hansen, Nanoscale Res. Lett. **10**, 67 (2015).

[63] L. Wang, V. Křápek, F. Ding, F. Horton, A. Schliwa, D. Bimberg, A. Rastelli, and O. G. Schmidt, Phys. Rev. B **80**, 085309 (2009).

[64] M. Jo, T. Mano, Y. Sakuma, and K. Sakoda, J. Cryst. Growth **378**, 5 (2013).

[65] B. Van Hattem, P. Corfdir, P. Brereton, P. Pearce, A. M. Graham, M. J. Stanley, M. Hugues, M. Hopkinson, and R. T. Phillips, Phys. Rev. B **87**, 205308 (2013).

[66] H. M. G. A. Tholen, J. S. Wildmann, A. Rastelli, R. Trotta, C. E. Pryor, E. Zallo, O. G. Schmidt, P. M. Koenraad, and A. Y. Silov, Phys. Rev. B **94**, 245301 (2016).

[67] A. Ulhaq, Q. Duan, E. Zallo, F. Ding, O. G. Schmidt, A. I. Tartakovskii, M. S. Skolnick, and E. A. Chekhovich, Phys. Rev. B **93**, 165306 (2016).

[68] N. Ares, V. N. Golovach, G. Katsaros, M. Stoffel, F. Fournel, L. I. Glazman, O. G. Schmidt, and S. De Franceschi, Phys. Rev. Lett. **110**, 046602 (2013).

[69] H. Watzinger, C. Kloeffel, L. Vukušić, M. D. Rossell, V. Sessi, J. Kukučka, R. Kirchschlager, E. Lausecker, A. Truhlar, M. Glaser, A. Rastelli, A. Fuhrer, D. Loss, and G. Katsaros, Nano Lett. **16**, 6879 (2016).

[70] R. J. Warburton, B. T. Miller, C. S. Dürr, C. Bödefeld, K. Karrai, J. P. Kotthaus, G. Medeiros-Ribeiro, P. M. Petroff, and S. Huant, Phys. Rev. B **58**, 16221 (1998).

[71] S.-J. Cheng, W. Sheng, and P. Hawrylak, Phys. Rev. B **68**, 235330 (2003).

[72] P. A. Dalgarno, J. M. Smith, J. McFarlane, B. D. Gerardot, K. Karrai, A. Badolato, P. M. Petroff, and R. J. Warburton, Phys. Rev. B **77**, 245311 (2008).

[73] C. Teichert, M. G. Lagally, L. J. Peticolas, J. C. Bean, and J. Tersoff, Phys. Rev. B **53**, 16334 (1996).

[74] G. Springholz, V. Holy, M. Pinczolits, and G. Bauer, Science **282**, 734 (1998).

[75] M. Pinczolits, G. Springholz, and G. Bauer, Phys. Rev. B **60**, 11524 (1999).

[76] N. Gogneau, F. Fossard, E. Monroy, S. Monnoye, H. Mank, and B. Daudin, Appl. Phys. Lett. **84**, 4224 (2004).

[77] S. Kiravittaya, A. Rastelli, and O. G. Schmidt, Appl. Phys. Lett. **88**, 043112 (2006).

[78] G. Biasiol, V. Baranwal, S. Heun, M. Prasciolu, M. Tormen, A. Locatelli, T. Mentes, M. Nino, and L. Sorba, J. Cryst. Growth **323**, 176 (2011).

[79] A. Mohan, P. Gallo, M. Felici, B. Dwir, A. Rudra, J. Faist, and E. Kapon, Small **6**, 1268 (2010).

[80] A. Pimpinelli and T. L. Einstein, Phys. Rev. Lett. **99**, 226102 (2007).

[81] M. A. Groce, B. R. Conrad, W. G. Cullen, A. Pimpinelli, E. D. Williams, and T. L. Einstein, Surf. Sci. **606**, 53 (2012).

[82] D. L. González, A. Pimpinelli, and T. L. Einstein, Phys. Rev. E **84**, 011601 (2011).

[83] T. L. Einstein, A. Pimpinelli, and D. L. González, J. Cryst. growth **401**, 67 (2014).

[84] A. Pimpinelli, L. Tumbek, and A. Winkler, J. Phys. Chem. Lett. **5**, 995 (2014).

[85] R. J. Rossi, *Mathematical Statistics: An Introduction to Likelihood Based Inference* (Wiley Online Library, 2018).